solid earth. Again the patterns in the Southern Hemisphere are more zonally uniform than in the Northern Hemisphere, as would be expected from the greater homogeneity of the earth's surface in that hemisphere. We should mention that the westerly winds between about 50 and 70 °S are probably underestimated due to poor data coverage over the southern oceans (see Fig. 5.3). The data gaps may also be a contributing factor in making the patterns in the Southern Hemisphere more uniform. The major contributions to the zonal momentum in the Northern Hemisphere stem from the midlatitude jets over eastern North America, Asia, and the adjacent oceans.

There are seasonal shifts of about 10° latitude in the belt of westerlies toward the summer pole. The westerlies are strongest in the winter hemisphere related to the increase in the pole-equator temperature gradient. These seasonal shifts can be inferred from the difference map in Fig. 7.14(b) and are also seen in the mean profiles of Fig. 7.20 (to be discussed in more detail later). The largest seasonal differences in the $\bar{u}_{200}$ field are located near 30° latitude in both hemispheres.

7.4.3 Vertical structure of the circulation

The vertical and meridional distributions of the mean zonal flow are presented in Fig. 7.15 with, on the right-hand side, vertical profiles of hemispheric and global mean conditions. The similarities between the two hemispheres for the annual mean are quite striking. For example, the zonal circulation in both hemispheres is dominated by a westerly jet maximum of about 25 m s^{-1} near 200 mb. However, there are also differences since in the Southern Hemisphere the winds at all levels between 35° and 60° latitude are consistently stronger, by about 5 m s^{-1}, than in the Northern

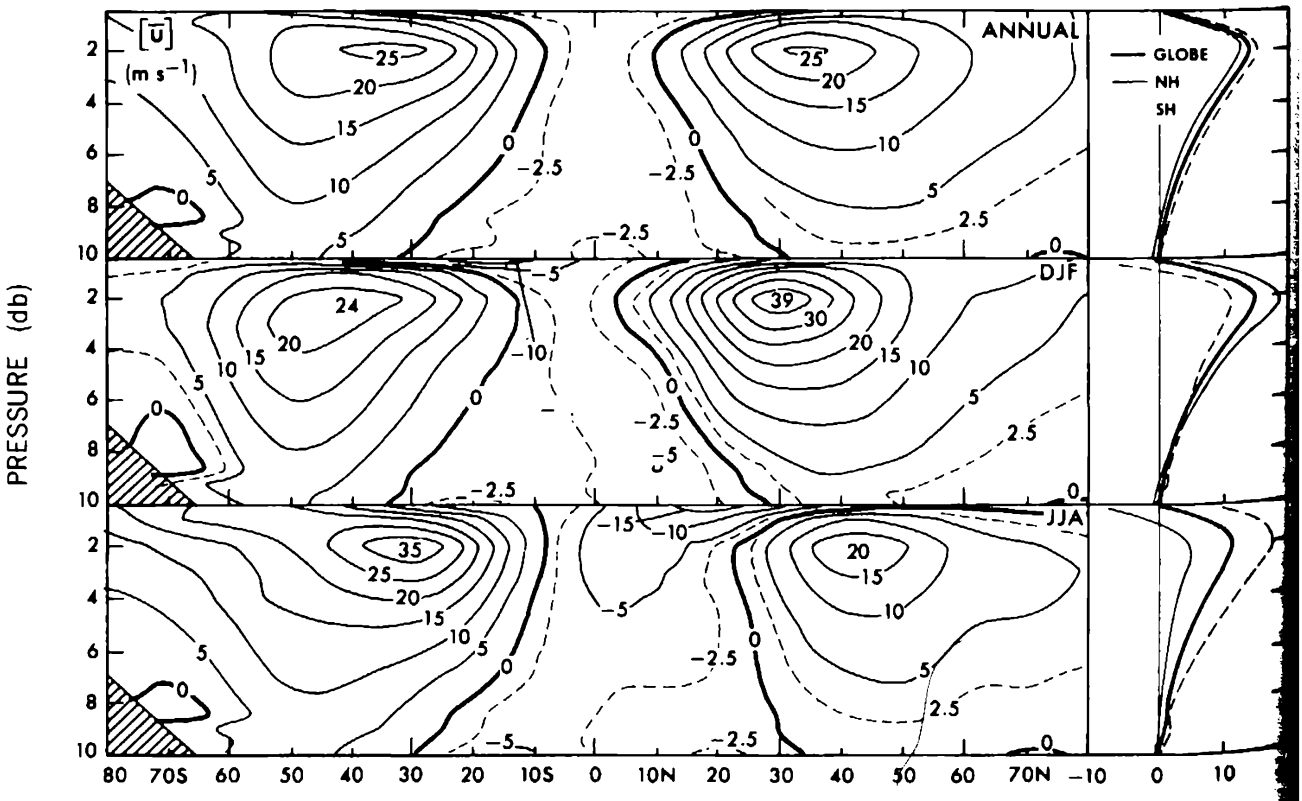

FIGURE 7.15. Zonal-mean cross sections of the zonal wind component in m s^{-1} for annual, DJF, and JJA mean conditions. Vertical profiles of the hemispheric and global mean values are shown on the right.

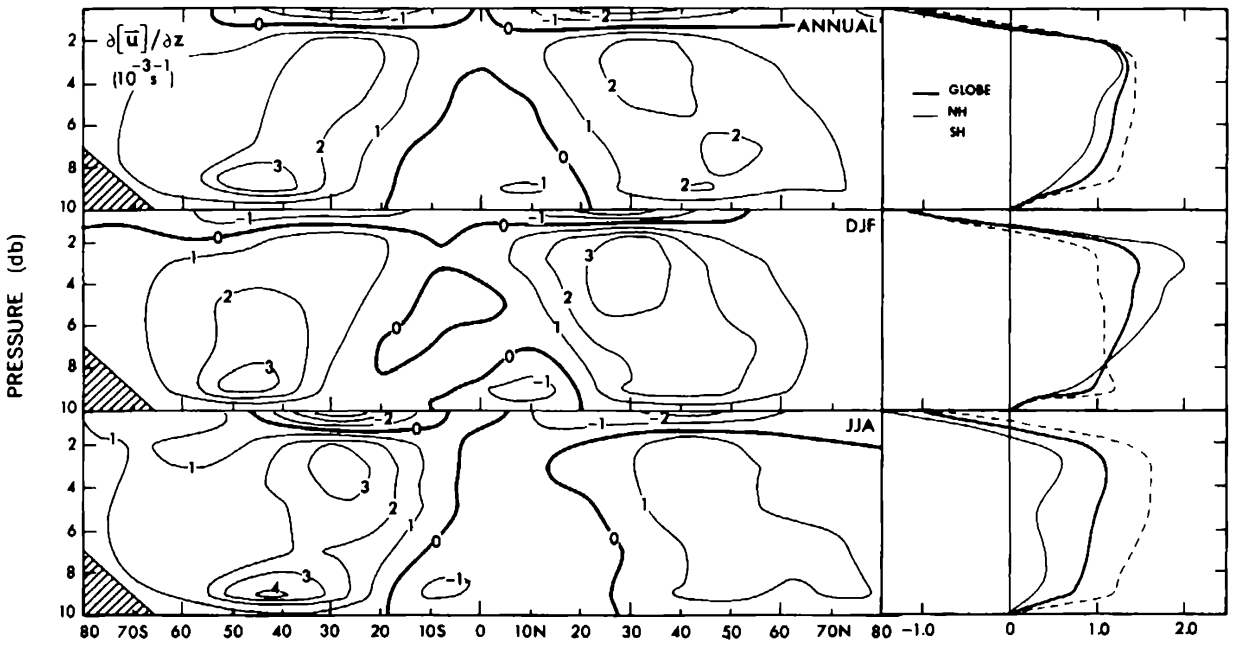

FIGURE 7.16. Zonal-mean cross sections of the vertical gradient of the zonal wind component (in 10^{-3} s^{-1}) for annual, DJF, and JJA mean conditions. Vertical profiles of the hemispheric and global mean values are shown on the right.

Hemisphere, reflecting the greater strength of the zonal winds in the Southern Hemisphere. Yet the winds in the Southern Hemisphere high latitudes should still be somewhat stronger than our analyses indicate because of the occurrence of large data gaps over the oceans and the bias due to a possible, selective loss of balloons during strong winds at some stations in the Southern Hemisphere [see the geostrophic wind estimates by Van Loon *et al.* (1971), Swanson and Trenberth (1981), and Oort (1983)]. Figure 7.15 also shows that easterly winds dominate in the tropical regions. The relatively weak surface easterlies in the equatorial zone are associated with the doldrums.

We further find that the surface easterlies and westerlies occupy almost equal areas and that, therefore, the global surface integrals are close to zero. We shall come back to this in the angular momentum discussion in Chap. 11. The broad maxima in $[\bar{u}]$ near 200 mb are located just above the regions where the north–south temperature gradient (i.e., the baroclinicity of the atmosphere) is a maximum.

A cross section of the vertical wind shear, $\partial[\bar{u}]/\partial z$, is shown in Fig. 7.16. Since, in general, the winds vary with height we can define a fictitious vector $\mathbf{v}_T$, the so-called thermal wind, so that $\mathbf{v}_T \equiv \mathbf{v}(z + \Delta z) - \mathbf{v}(z) \approx (\partial \mathbf{v}/\partial z)\Delta z$. As we will show next, the vertical shear is related to the temperature gradient through the thermal wind equation. This equation can be derived assuming that the horizontal flow is geostrophic (see Eq. 3.15). The shear is then given by

$$\frac{\partial}{\partial z}(\rho \mathbf{v}_g) = \frac{1}{f}\mathbf{k} \times \text{grad}\, \frac{\partial p}{\partial z}$$

or with the hydrostatic approximation (3.13)

$$\frac{\partial \mathbf{v}_g}{\partial z} = -\frac{g}{\rho f}\mathbf{k} \times \text{grad}\, \rho - \frac{1}{\rho}\frac{\partial \rho}{\partial z}\mathbf{v}_g.$$

Using the equation of state after logarithmic differentiation and again Eq. (3.15), we obtain finally for the wind shear vector

$$\frac{\partial \mathbf{v}_g}{\partial z} = \frac{g}{f}\mathbf{k} \times \frac{\text{grad}\, T}{T} + \frac{1}{T}\frac{\partial T}{\partial z}\mathbf{v}_g. \tag{7.6a}$$

Scale analysis of the last equation, the thermal wind equation, for large-scale flow shows that the first term on the right hand side dominates so that

$$\frac{\partial \mathbf{v}_g}{\partial z} \approx \frac{g}{fT} \mathbf{k} \times \text{grad } T. \tag{7.6b}$$

Thus the vertical shear at a given level is proportional to the gradient of temperature and parallel to the isotherms. The geostrophic wind will increase with height ($\partial \mathbf{v}_g / \partial z > 0$) with the warm air on the right of the shear vector in the Northern Hemisphere and on the left in the Southern Hemisphere.

The thermal wind equation (7.6b) can be also written in the p-system in terms of the potential temperature θ using Eq. (3.47):

$$\frac{\partial \mathbf{v}_g}{\partial p} \approx -\frac{1}{\rho\theta} \mathbf{k} \times \text{grad } \theta. \tag{7.6c}$$

According to the thermal wind equation, the zonal wind increases with height [$\partial u_g / \partial z \approx -(g/fT)(\partial T / R\partial\phi) > 0$] in midlatitudes where the meridional temperature gradient is most pronounced. Of course, in regions where the atmosphere is barotropic the winds do not change with height ($\mathbf{v}_T = 0$) because grad $T = 0$ (see Sec. 3.5.3). However, Fig. 7.16 shows that the atmosphere is in general baroclinic.

Let us show how the thermal wind is related to the baroclinicity vector **N** (see Sec. 3.5.3). If we take the cross product of **N** with the vertical unit vector **k** we find

$$\mathbf{k} \times \mathbf{N} = -\frac{1}{\rho T} (\mathbf{k} \cdot \text{grad } p) \text{grad } T + \frac{1}{\rho T} (\mathbf{k} \cdot \text{grad } T) \text{grad } p.$$

Using the hydrostatic approximation this equation becomes

$$\mathbf{k} \times \mathbf{N} = \frac{g}{T} \text{grad } T + \frac{1}{\rho T} \frac{\partial T}{\partial z} \text{grad } p.$$

If we again cross multiply with **k** we find

$$\mathbf{k} \times (\mathbf{k} \times \mathbf{N}) \equiv -\mathbf{N} + N_z \mathbf{k} = \frac{g}{T} \mathbf{k} \times \text{grad } T + \frac{1}{\rho T} \frac{\partial T}{\partial z} \mathbf{k} \times \text{grad } p.$$

Using the geostrophic wind equation (3.15) and the thermal wind equation (7.6a), noting that $\mathbf{N}_h = \mathbf{N} - N_z \mathbf{k}$ is the horizontal vector component of **N**, we find

$$-\mathbf{N}_h = \frac{g}{T} \mathbf{k} \times \text{grad } T + \frac{f}{T} \frac{\partial T}{\partial z} \mathbf{v}_g = f \frac{\partial \mathbf{v}_g}{\partial z}.$$

Of course, $\mathbf{N}_h$ represents the number of solenoids in a vertical plane across the solenoidal tubes and measures the baroclinicity in that plane. Thus, as we have seen before, in a barotropic atmosphere ($\mathbf{N}_h = 0$) the winds do not change with height.

The meridional component of the zonal-mean circulation is shown in Fig. 7.17. Outside the tropics the evaluation of the mean meridional circulation from the observed $\bar{v}$ field becomes unreliable and even unusable in the Southern Hemisphere. In view of this difficulty, we have used indirectly computed values of $[\bar{v}]$ poleward of 15° latitude, in both hemispheres (see Oort and Peixoto, 1983). For the region between 15 °S and 15 °N, the directly measured $[\bar{v}]$ values were used because there the time-mean meridional winds are fairly uniform and the observational network seems ade-

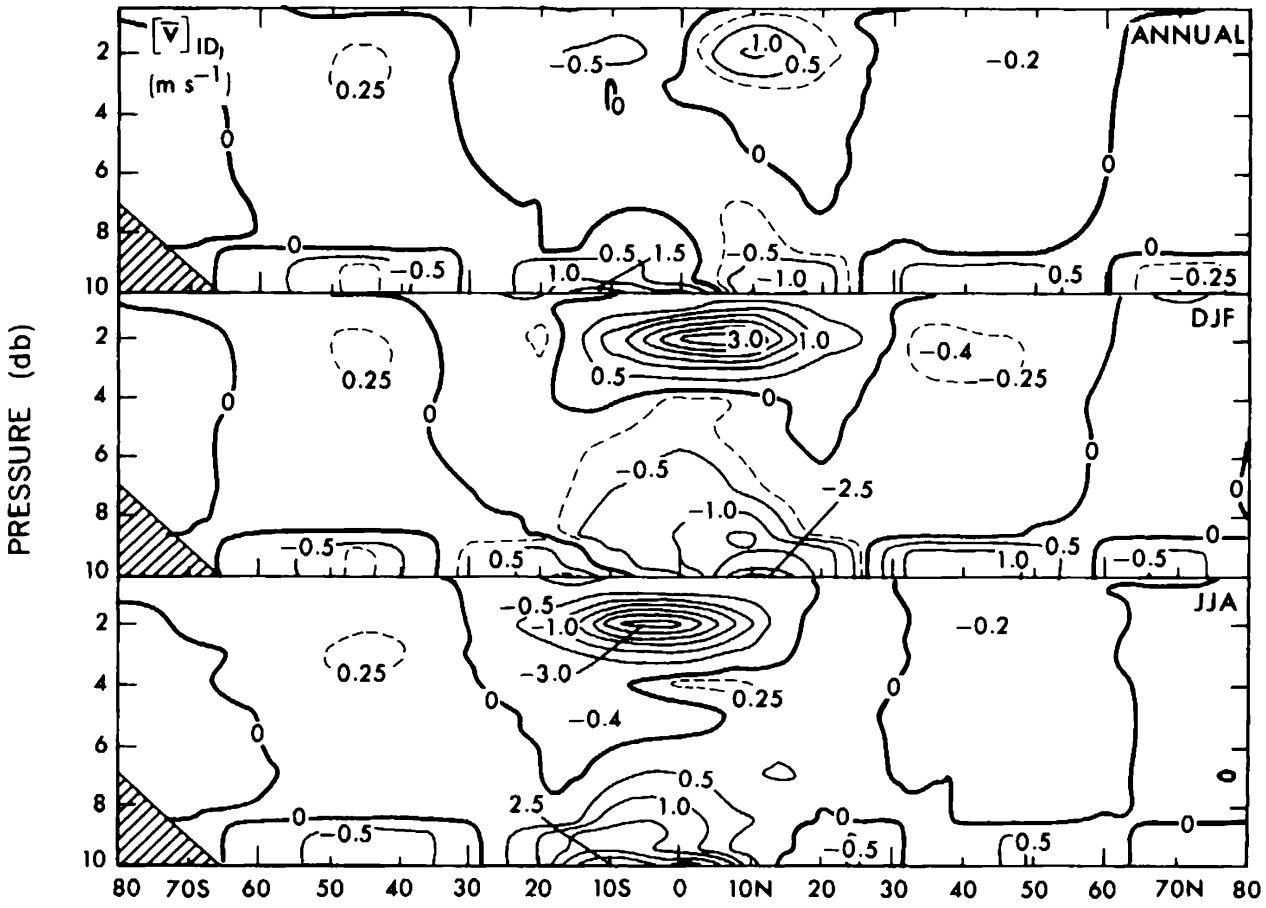

FIGURE 7.17. Zonal-mean cross sections of the meridional wind component in m s $^{-1}$ for annual, DJF, and JJA mean conditions. The $[\bar{v}]$ values between 10° S and 10° N were computed directly from the rawinsonde analyses, and poleward of 20° latitude indirectly from momentum balance.

quate to monitor the dominant zonally symmetric circulation. Between 10° and 20° latitude the values derived from the two methods were averaged with weights varying between 0 and 1.

Although small, the meridional component of the wind plays an important role in maintaining the zonal winds [fv term in the zonal equation of motion (3.18a)]. The lower branches of the tropical Hadley circulations are directly associated with the northeast and southeast trade winds, whereas the lower branches of the Ferrel cells are associated with the prevailing westerlies in midlatitudes, and those of the polar cells with the polar easterlies.

Cross sections of the vertical velocity $[\bar{\omega}]$ can be computed from the $[\bar{v}]$ values in Fig. 7.17 using the continuity equation of mass in zonally averaged form (7.7) and the streamfunction approach (7.8) to be discussed next. The resulting vertical velocity patterns in Fig. 7.18 show for the annual-mean strong rising motions of 2×10^{-4} mb s^{-1} (or about 3 mm s^{-1}) centered near 5 °N, associated with the mean position of the ITCZ. This equatorial belt is flanked in each hemisphere by sinking motions between about 10° and 40° latitude, followed by rising motions between 50° and 70° latitude, and weak sinking motions poleward of 70° latitude. In northern winter we find the strongest rising motions between 10 °N and 20 °S and the strongest sinking motions between 10 and 35 °N, whereas in northern summer the strongest rising motions are found between 10 °S and 20 °N and the strongest sinking motions between 10 and 40 °S. The vertical profiles on the right-hand side of Fig. 7.18 are basically symmetric for both hemispheres with a sign reversal between winter and summer. Extreme values occur between about 400 and 500 mb.

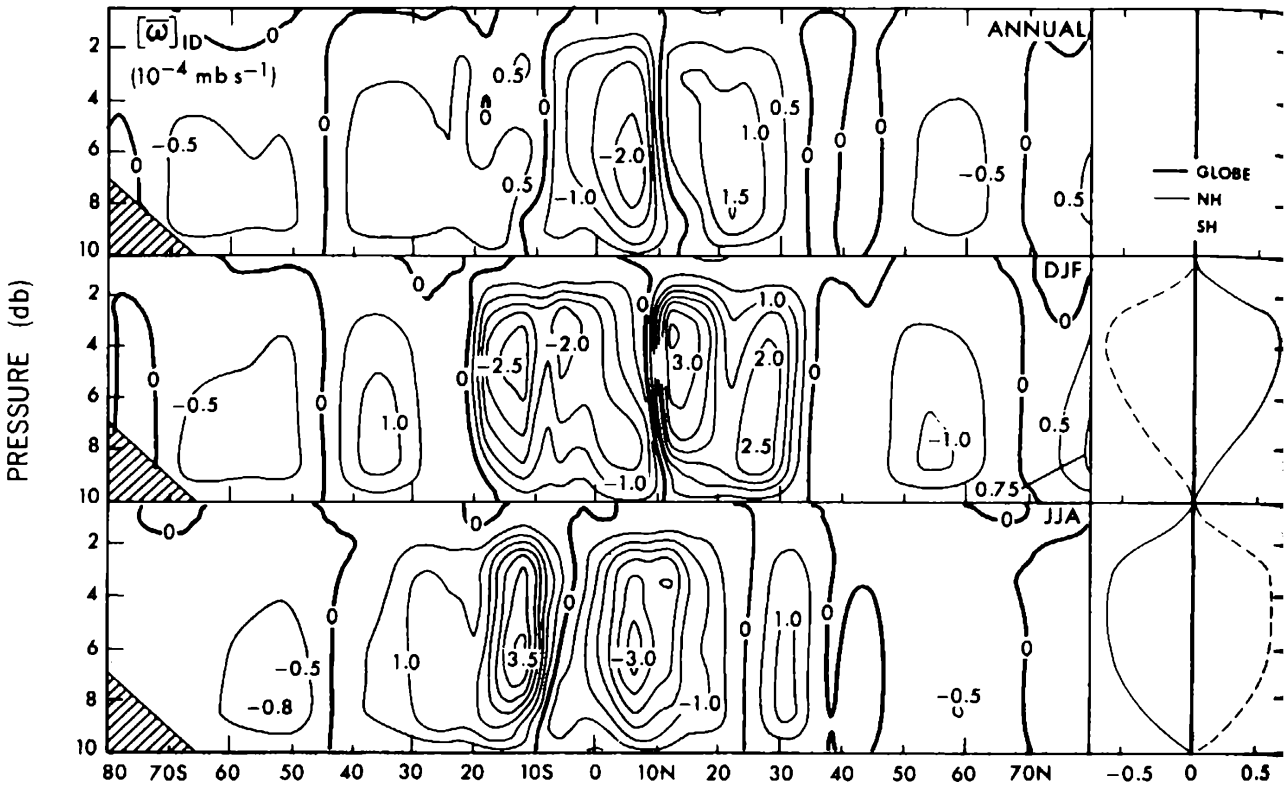

FIGURE 7.18. Zonal-mean cross sections of the vertical velocity ω in 10^{-4} mb s^{-1} for annual, DJF, and JJA mean conditions as computed from the meridional velocities in Fig. 7.17 using conservation of mass. Vertical profiles of the hemispheric and global mean values are shown on the right.

The $[\bar{v}]$ data can also be used to construct streamlines indicating the mean overturnings of mass in a north–south cross section. A stream function can be computed using the continuity equation of mass (3.4) in zonally averaged form:

$$\frac{\partial[\bar{v}]\cos\phi}{R\cos\phi\partial\phi} + \frac{\partial[\bar{\omega}]}{\partial p} = 0. \tag{7.7}$$

Thus, we may introduce the so-called Stokes stream function ψ given by the equations

$$[\bar{v}] = g\frac{\partial\psi}{2\pi R\cos\phi\partial p}, \tag{7.8a}$$

$$[\bar{\omega}] = -g\frac{\partial\psi}{2\pi R^2\cos\phi\partial\phi}. \tag{7.8b}$$

We can now calculate the ψ field from the observed $[\bar{v}]$ distribution by vertical integration of Eq. (7.8a) starting at the top of the atmosphere where we assume that $\psi = 0$. The meridional gradient of ψ then gives the vertical component $[\bar{\omega}]$ of the zonally symmetric overturnings.

The computed annual-mean and seasonal streamlines are shown in Fig. 7.19. The circulation cells in these cross sections are often called "mean meridional circulations." It is clear that the annual-mean cells in the tropics represent an average of two very different winter and summer patterns, and that they are perhaps only representative for conditions during the transition seasons in spring and fall. The annual-mean picture thus shows a somewhat idealized situation of three cells in each hemisphere, one in the tropical regions (the so-called Hadley cell), another in midlatitudes (the Ferrel cell), and finally a third one in the polar regions (the polar cell).

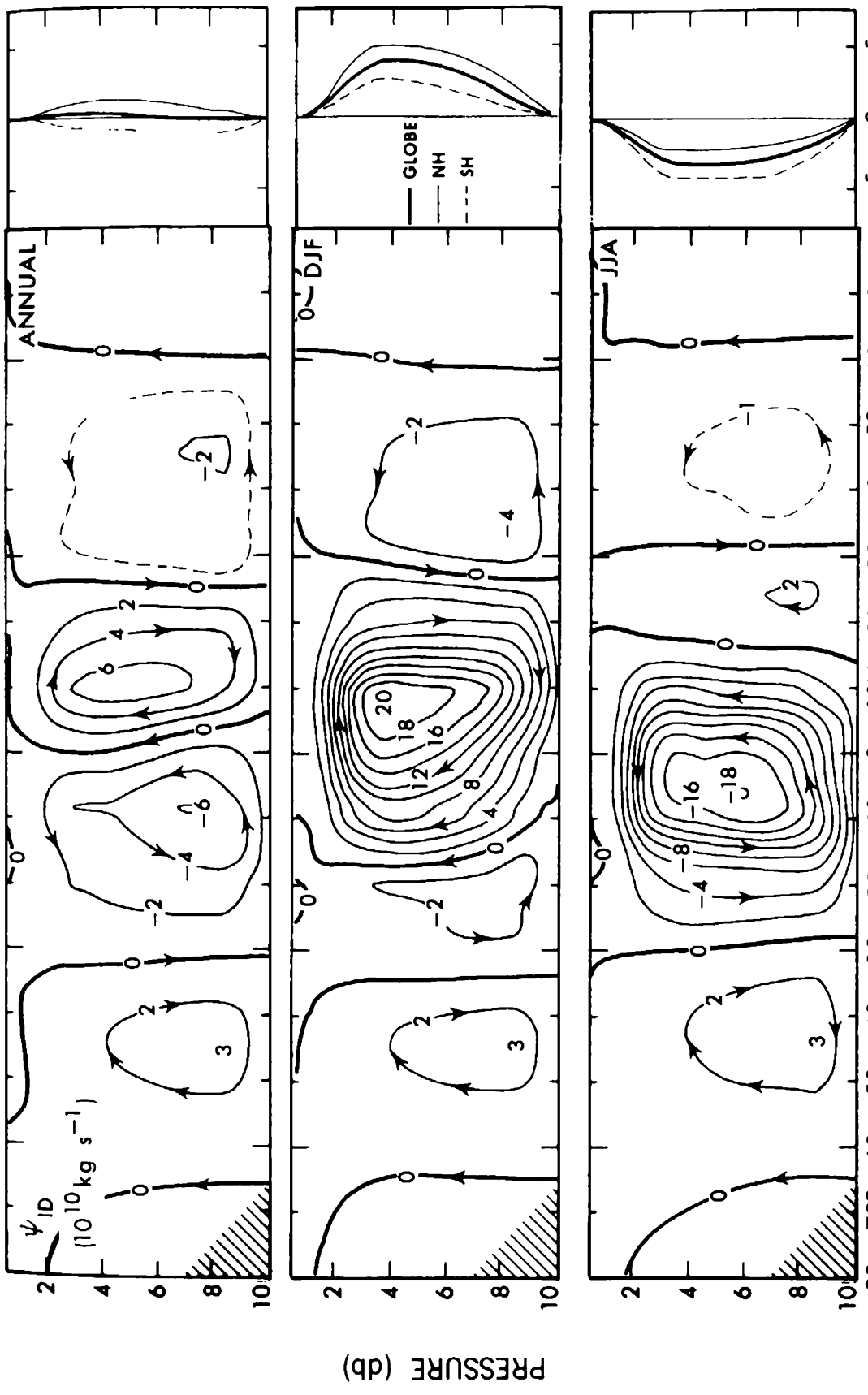

FIGURE 7.19. Zonal-mean cross sections of the mass stream function in 10^{10} kg s^{-1} for annual, DJF, and JJA mean conditions. Vertical profiles of the hemispheric and global mean values are shown on the right.

The seasonal cross sections presented in Fig. 7.19 are very interesting because they show the strong intensification and predominance of the winter Hadley cell and the almost disappearance of the summer Hadley cell in each hemisphere. The intensification leads to a shift of the low-level circulation into the summer hemisphere. The Ferrel cells also appear to be more intense in the winter season, the differences being more pronounced in the Northern Hemisphere as one would expect. The vertical profiles on the right-hand side of Fig. 7.19 reflect the seasonal behavior of the Hadley cells, and show the antisymmetry of the profiles between the two seasons.

The direct Hadley cells in the tropics in the three cross sections of Fig. 7.19 are much stronger than the indirect Ferrel cells in middle latitudes. At these latitudes the circulation is dominated by almost horizontal, wave-like flows, and the Ferrel cells are only small statistical residues which result after zonal averaging of large, almost compensating, northward and southward flows in the quasistationary atmospheric waves. The direct polar cells are quite weak. In the annual mean, the southern Hadley cell penetrates across the equator reinforcing the upward motions characteristic of the mean ITCZ.

In the Hadley cells, there is a rising of warm (light) and moist air in the equatorial region and a descent of colder (heavier) air in the subtropics leading to a thermally driven direct circulation. However, in the Ferrel cells there is a rising of relatively cold air in high latitudes and a sinking of relatively warm air in the lower midlatitudes leading to a thermally indirect circulation in which cold air is forced to rise. In a direct circulation with the lowering of the center of mass there is a production of kinetic energy, whereas in an indirect cell with the net rising of the center of mass there is a consumption of kinetic energy. Further discussions on the mean meridional circulations and their maintenance will be given in Sec. 14.5.

The vertical motion patterns associated with the mean meridional circulations also indicate the principal climate zones, namely the equatorial rainy zone, the subtropical arid and desert-like zones, the moist mid to high-latitude zones, and the dry polar zones.

As a final remark, we want to emphasize that the observed three-cell regime in the annual-mean atmosphere results, of course, from the imposed pole-to-equator gradient in net radiation combined with the rotation of the earth. For different rotation rates, such as is the case for the other planets, we can expect a different number and configuration of cells. For example, in the low-rotation case, we may have one direct cell in each hemisphere as Hadley proposed in 1735 to explain the trade winds, while in the high-rotation case we may have many more cells such as may occur for Jupiter (see, e.g., Williams and Holloway, 1982).

7.4.4 Variability of the circulation

To show the temporal and spatial variability of the wind components, profiles of the vertical- and zonal-mean standard deviations for u and v are presented in Fig. 7.20.

It is of interest to mention the close symmetry between the two hemispheres. Further, for both u and v the temporal standard deviations are of the same magnitude as $[\bar{u}]$ or even larger at certain latitudes. This feature, as well as the nearly identical patterns for the temporal standard deviations of u and v, clearly point out the turbulent character of the atmospheric general circulation. The larger winter–summer contrast in the $\sqrt{\overline{u'^2}}$ curves in the Northern Hemisphere reflects the larger variability of the northern jet streams. In terms of the transient eddy kinetic energy